Strain, magnetic anisotropy, and composition modulation in hybrid metal–oxide vertically assembled nanocomposites

Marcel Hennes, Dominique Demaille, Gilles Patriarche, Thomas Tran, Yunlin Zheng, Franck Vidal

Strain, magnetic anisotropy and composition modulation in hybrid metal-oxide vertically assembled nanocomposites

Marcel Hennes, Dominique Demaille, Gilles Patriarche, Thomas Tran, Yunlin Zheng, Franck Vidal (*)

Marcel Hennes
Laboratoire de Chimie Physique - Matière et Rayonnement, Sorbonne Université, CNRS UMR 7614, 4 place Jussieu, Tour 43/44, Etage 1, 75252 Paris Cedex 05, France
Dominique Demaille, Thomas Tran, Yunlin Zheng, Franck Vidal*
Institut des NanoSciences de Paris, Sorbonne Université, CNRS UMR 7588, BC 840 - 4 place Jussieu 75252 Cedex 05 Paris, France
* Email: franck.vidal@sorbonne-universite.fr
Gilles Patriarche
Université Paris-Saclay, CNRS, Centre de Nanosciences et de Nanotechnologies, 91120, Palaiseau, France

Self-assembled vertically aligned nanocomposites (VANs) have recently emerged as a novel playground for strain engineering of physical properties in nanostructures. In contrast to thin films obtained by classical planar heteroepitaxy, VANs consist of two (or more) intertwined phases, coupled along vertical interfaces. Their unique nanoarchitecture, which can be tuned by choosing appropriate growth conditions, allows to achieve and stabilize deformations that cannot be easily attained in traditional flat geometries. In the present contribution, we show how nanometer-sized acicular inclusions of magnetic 3d metals in various oxide host matrices can be obtained via sequential pulsed laser deposition and demonstrate how to use strain, to accurately control the magnetic anisotropy of this type of metal-oxide VANs. We eventually discuss possible extensions of

this approach to more than one embedded metallic phase, which might pave the way for the creation of hybrid magnetoplasmonic devices.

Keywords: nanostructure, ferromagnetic, plasmonic, composite, laser ablation.

Introduction

VANs are nanocomposite systems made of nanowires (NWs) epitaxially coupled to a surrounding matrix (Figure 1a). While early work on these hybrid thin films already demonstrated the possibility to grow embedded metallic nanostructures[1], most of the subsequent research focused essentially on all oxide VANs (oxide-oxide VANs). Especially the combination of perovskite and spinel oxides has attracted tremendous attention and led to major advances in the development of multiferroic nanocomposites[2-7]. In recent years however, the interest for hybrid VANs composed of an oxide matrix and embedded nanowires made of transition or noble metals (metal-oxide VANs) has grown considerably[8-27]. These systems naturally offer some advantages that may lead to advances in a variety of fields such as nanomagnetism, or plasmonics.

Growth and structural properties of metal-oxide VANs

The growth of epitaxial metal-oxide VANs is based on self-assembly mechanisms driven by metal-oxide phase segregation during synthesis. Pulsed laser deposition is particularly suitable to obtain the desired metal-oxide structures, allowing for deposition at high temperature (>600°C) and under high vacuum conditions (<10^{-5} mbar). VANs can be grown from a single target containing oxide components[1] or by using a multi-target approach based on the alternating deposition of the metallic and oxide species[12,14]. Such sequential growth schemes generally rely on the repetition of one basic sequence where submonolayer amounts of the materials are deposited. This offers precise control over the composition. CoNi-$SrTiO_3$ VANs for example can be grown by shooting alternatively on CoO, NiO and $SrTiO_3$ (STO) targets. The NW diameter and volume fraction in the epilayer can then be controlled by the ratio of the number

of shots on CoO-NiO targets and on the STO target[12,14]. The Co content in the NWs is tuned by the ratio of the shots on CoO and NiO. The epilayer thickness, thus the NW length, results from the total number of basic sequences. With this procedure, arrays of ultrathin (diameter < 5 nm) Co, Ni and CoNi alloy NWs with high densities (> 10^{11} cm^{-2}) have been obtained.

VAN growth mechanisms are complex, as they involve simultaneous phase segregation, nucleation and coalescence phenomena in oxide and metallic phases. However, the initial stages of VAN self-assembly can be grasped by using appropriate computer simulation approaches. Ni-STO VAN thin film deposition was for example successfully described using a coarse-grained kinetic Monte-Carlo scheme[21] which allowed to identify the parameters affecting the final assembly. While low growth temperatures result in short, isolated Ni nano-inclusions in the matrix, increasing the deposition temperature beyond 820 K favors the growth of rods. Systematic increase of the Ni/STO ratio in a basic sequence yields larger average NW diameters, while the overall wire density remains constant. The relaxation time between deposition steps also constitutes a key parameter to accurately tune the NW size and density.

One central feature of VANs is the epitaxial NW/matrix coupling along the vertical interface resulting in strained NWs[28], which permits to overcome the conventional critical thickness for strain relaxation in planar heterostructures, as discussed by MacManus-Driscoll *et al.* and Chen *et al.* in oxide-oxide VANs[29-30]. In metal-oxide VANs, the dilation along the nanowire backbone can reach several percent when choosing appropriate metal/oxide combinations: In Ni-CeO_2 VAN thin films[13] for example, an axial tensile strain of 1.5% was reported. In highly lattice-mismatched systems such as CoNi-(BaSr)TiO_3[14] or CoNi-STO[27], the latter can even reach up to 4%, as shown in Figure 2a and 2b, while the radial compressive strain remains negligible.

As the NW/matrix interface energy scales with the NW diameter ($\sim d$) while the volume elastic energy scales with its sectional area ($\sim d^2$), the axial strain in NWs increases when the diameter decreases (Figure 2a). Calculations using a Frenkel-Kontorova toy model[13] indicate that the tensile strain state observed in

NWs is metastable and that the sequential growth scheme, with progressive adaptation of NW atoms to local variations of the periodic matrix potential, plays an important role in stabilizing the large axial strains. However, the actual strain state is more complex than what can be predicted using this simplified 1D approach which only takes the horizontal (001) lattice planes into account. In fact, (101) and (111) dense planes also play an important role in imposing a lattice and orientation matching between segments of a NW and the matrix[22,27]. Beyond the mean axial strain observed, partially relaxed segments were identified in NWs, with (101) and (111) planes almost parallel to those of the matrix and further relaxed segments in Ni NWs, with a small rotation around [100]-type axis. Figure 2c shows a cross-sectional transmission electron microscopy image of a Ni-STO VAN, unraveling local tilts of 4°. Such a rotation leads to lattice matching along the NW/matrix vertical heterointerface for one set of (101) planes, but it also results in an increase of structural disorder[22]. In ultrathin wires, these complex structural rearrangements ultimately lead to an almost complete loss of crystalline structure[22]. Strain relaxation mechanisms in metal/oxide VANs thus differ from their all oxide counterparts, where substitutional defect formation, misfit dislocations and antiphase boundaries were often reported[31].

Tailoring the magnetic anisotropy in metal-oxide VANs

The magnetic anisotropy K is a key property of nanomagnets because it determines the direction of easy magnetization and the temperature range of stability of the magnetization. VANs are ideal systems for tailoring the magnetic anisotropy. Indeed, as shown schematically in Figure 1, by tuning the growth parameters, and thus the final nanoarchitecture of the VANs, it is possible to control the distinct sources of K independently.

The shape of the embedded nanopillars offers direct control over the magnetostatic part of K, the so-called shape anisotropy K_{ms}. This contribution scales with the square of the magnetization M_s and is given, in the case of nanowires with large aspect ratio, by:

$$K_{ms} = \mu_0 M_s^2/4. \quad (1)$$

Thus, using materials with a large value of M_s is a simple way to obtain a large uniaxial anisotropy. This has been shown for Fe nanopillars obtained by decomposition, as reported in the seminal work of Ref. 1. In such metal-oxide VANs, nanowires exhibited a robust ferromagnetic response at room temperature with a clear easy axis along their backbone and a large coercive field for aspect ratios larger than 5. More recently, the possibility to tune the shape of pillars, in particular their cross section, by adjusting the growth rate, was demonstrated for Fe-$BaTiO_3$ VANs[32] resulting in a tunable magnetization and coercivity.

The epitaxial relationship determines the orientation of the embedded nanocrystal and thus, the easy magnetic directions favored by the magnetocrystalline anisotropy K_{mc}. For most metals studied so far, this contribution has only played a minor role[27] and it remains to be fully elucidated, whether more complex metallic nanoalloys such as CoPt and FePt, exhibiting hard magnetic phases as a result of chemical short-range ordering, can be integrated into VANs.

Finally, the large axial strain within the nanopillars is a lever that can be used to tune the magnetoelastic anisotropy K_{me}. For a cubic structure and [001] direction parallel to the longitudinal axis, it is given by:

$$K_{me} = 3\lambda_{001}(c_{11}-c_{12})(\varepsilon_{zz}-\varepsilon_{rr})/2, \quad (2)$$

λ_{001} is the magnetostriction coefficient, c_{ij} are elastic constants, ε_{zz} and ε_{rr} are the axial and radial strain in the nanowires, respectively. In the case of VANs containing alloy nanowires (such as Co_xNi_{1-x}), one benefits from an additional degree of freedom: the composition of the metallic inclusions, adjusted precisely via the growth sequence: In pure Ni, λ_{001} is negative. In Co_xNi_{1-x} alloys, λ_{001} increases with x, reaches 0 around x=18% and is positive above this composition. Thus, by controlling both, the strain and the composition of Co_xNi_{1-x} nanowires, it becomes possible to obtain *à-la-carte* uniaxial magnetic anisotropies[12,14,24].

In pure Ni nanowires, there is a threshold value, ε_{crit}, for the axial strain that determines the transition from an easy magnetic axis along the axis of the wires to a hard axis. The value of ε_{crit} is determined by the competition of the shape anisotropy (**equation 1**) and the magneto-elastic anisotropy (**equation 2**). For Ni nanowires embedded epitaxially in a CeO_2 matrix (grown on $SrTiO_3$(001) substrate), the axial dilation is of the order of 1%, near ε_{crit}, and the system is nearly isotropic from a magnetic point of view[12]. In a $SrTiO_3$ matrix (grown on $SrTiO_3$(001) substrate), the strain in Ni nanowires is much larger, as shown in Figure 2a and one can expect a reversal of the magnetic behavior: the axis of the wires switches from easy to hard. This is indeed what has been observed[24], as demonstrated in Figure 3a-b. In Ni-STO VANs, the strain largely exceeds ε_{crit} and the axis of the wires becomes the hard axis with a minimal value of the remanence, as shown in Figure 3b.

In VANs incorporating Co_xNi_{1-x} nanowires, the axial strain is still large (see Figure 2b). Based on the above considerations, for *x* close to 18%, only the shape anisotropy is present in the system. This could indeed be verified by quantitative measurements of the magnetic anisotropy in $Co_{0.2}Ni_{0.8}$-(BaSr)TiO_3 VANs through a combination of cyclic magnetometry (figure 3c) and ferromagnetic resonance measurements[14]. For higher Co contents, the magnetoelastic contribution should lead to an enhancement of the uniaxial anisotropy. This was confirmed in Co_xNi_{1-x}-CeO_2 VANs: Figure 3d shows magnetic hysteresis cycles recorded at room temperature for a $Co_{0.63}Ni_{0.37}$-CeO_2 VAN exhibiting a ferromagnetic response with strongly anisotropic behavior. Extraction of the values of the effective uniaxial anisotropy, $K_{eff.}$ of the system shows that it indeed exceeds the shape anisotropy contribution at high Co content (Figure 3e).

The strain engineering approach thus enables to boost *K* and to push the superparamagnetic limit far beyond room temperature, even for NWs with diameters smaller than 5 nm. This is an exciting perspective for future data storage applications and might be a key step towards controlling anisotropic transport properties in VAN-based nano-devices[18].

Towards axial structuration and hybrid nanowires

Metal-oxide VANs with two distinct embedded metallic phases can yield additional appealing functionalities. Figure 4a illustrates some hypothetical nanoarchitectures, reminiscent of the multiple configurations adopted by bimetallic nanoparticles[33,34]. To what extent can these structures be predicted in real-world VANs? Simulation approaches have been developed during the last two decades and turned into powerful tools used to analyze bi- and trimetallic particle structures[35]. However, the integration of metal-oxide interactions into the calculations[36] remains a great challenge. So far, the theoretical analysis of phase separation tendencies in bimetallic VANs has remained limited to basic thermodynamic considerations[23].

Embedded structures with core-shell (CS) or multishell architecture provide an in-plane modulation of the wire properties. In freestanding NWs, such configurations have been extensively studied and result from sequential growth approaches, where the core of the NW is obtained first, then covered by the shell material. This is hardly compatible with VAN growth, where the wire and matrix assemble simultaneously. The growth of core-shell VANs is thus challenging. Most alternative approaches developed so far, such as post-growth annealing, yielded limited success. Partial interdiffusion at the NW/matrix vertical interface has been observed in oxide-oxide VANs[37] giving rise to a "diffuse" CS configuration. Spontaneous decomposition and segregation processes, occurring during growth, have been shown to lead to CS configurations (Cu core-SrO shell[38] and TiO core-MgO shell[39]) but, to the best of our knowledge, this has not been achieved with two embedded metallic phases.

With regard to their magnetic and charge/spin transport properties, backbone-concentration modulated magnetic NWs appear even more appealing than their CS counterparts. Combining for example soft and hard magnetic materials would allow the growth of self-organized spin-valves with unprecedented small diameters. At first sight, these structures seem less challenging to synthesize. One might for example expect to obtain multilayered

NWs (Figure 4a) upon sequential deposition of different metallic species. Unfortunately, the rather high growth temperatures required to achieve metal/oxide phase separation concomitantly induce pronounced vertical atom mobility. Working with miscible metals requires finding a compromise between in-plane[40] and out-of-plane diffusion[21], in order to avoid creation of a bimetallic solid solution. Mixing of the components can be avoided by choosing appropriate material combinations. Au-Co or Ag-Co for example remain fully immiscible in the solid phase, even in nanoscale structures. However, the equilibrium VAN configurations resulting from co-deposition of these metals are also strongly influenced by differences in their surface energy. Co-growth of Au-Co-STO and Ag-Co-TiO_2 produced bilayered NWs, with the component with lower surface energy located at the NW top[23,41,42]: Au and Ag act as metallic surfactants, pushing incoming Co atoms to the bottom of the NW (Figure 4b), which additionally minimizes the interface between the two immiscible metallic phases. Similar processes have also been observed in three-phase metal/oxide/oxide composites[43].

While this impedes the growth of multilayer NWs, the aforementioned noble metals - ferromagnetic bilayer configurations can still be considered highly promising for a variety of applications, especially with regard to their plasmonic functionalities. The potential of self-assembly to yield embedded metallic columns with tunable optical resonances has been recognized early on[44,45] and was recently renewed for VANs[16,46]. Coupling of these plasmonic features with magnetic properties might turn VANs into a beautiful playground for magnetophotonic studies at the nanoscale[47], especially in an ultrafast regime[48], where fascinating non-equilibrium phenomena such as sub-ps demagnetization[49] and all optical switching[50] can be triggered by optical fs-pulses.

Summary and outlook

Metal-oxide VANs constitute a novel class of hybrid thin films of special interest in the field of nanomagnetism, providing the opportunity to obtain *à-la-carte* magnetic anisotropies. Among the challenges ahead, the successful growth of

modulated multi-metallic VANs structures, combining distinct physical properties, will be of utmost interest in the emerging field of magnetoplasmonics. Bimetallic VANs would be an ideal playground to study novel synergy effects on ultrashort timescales, thereby paving the way for an improved photon-based control of magnetic properties in ferromagnetic nanomaterials.

References

1. L. Mohaddes-Ardabili, H. Zheng, S. B. Ogale, B. Hannoyer, W. Tian, J. Wang, S. E. Lofland, S. R. Shinde, T. Zhao, Y. Jia, L. Salamanca-Riba, D. G. Schlom, M. Wuttig, R. Ramesh, *Nat. Mater.* **3**, 533 (2004).

2. H. Zheng, J. Wang, S. E. Lofland, Z. Ma, L. Mohaddes-Ardabili, T. Zhao, L. Salamanca-Riba, S. R. Shinde, S. B. Ogale, F. Bai, D. Viehland, Y. Jia, D. G. Schlom, M. Wuttig, A. Roytburd, R. Ramesh, *Science* **303**, 661 (2004).

3. N. Dix, R. Muralidharan, J.-M. Rebled, S. Estradé, F. Peiró, M. Varela, J. Fontcuberta, F. Sánchez, *ACS Nano* **4**, 4955 (2010).

4. N. M. Aimon, D. H. Kim, H. K. Choi, C. A. Ross, *Appl. Phys. Lett.* **100**, 092901 (2012).

5. W. Zhang, J. Jian, A. Chen, L. Jiao, F. Khatkhatay, L. Li, F. Chu, Q. Jia, J. L. MacManus-Driscoll, H. Wang, *Appl. Phys. Lett.* **104**, 062402 (2014).

6. H.-J. Liu, Y.-Y. Liu, C.-Y. Tsai, S.-C. Liao, Y.-J. Chen, H.-J. Lin, C.-H. Lai, W.-F. Hsieh, J.-Y. Li, C.-T. Chen, Q. He, Y.-H. Chu, *Sci. Rep.* **5**, 12073 (2015).

7. T. O. Farmer, E.-J. Guo, R. D. Desautels, L. DeBeer-Schmitt, A. Chen, Z. Wang, Q. Jia, J. A. Borchers, D. A. Gilbert, B. Holladay, S. K. Sinha, and M. R. Fitzsimmons, *Phys. Rev. Materials* **3**, 081401(R) (2019).

8. F. Vidal, Y. Zheng, J. Milano, D. Demaille, P. Schio, E. Fonda, B. Vodungbo, *Appl. Phys. Lett.* **95**, 152510 (2009).

9. P. Schio, F. Vidal, Y.Zheng, J. Milano, E. Fonda, D. Demaille, B. Vodungbo, J.Varalda, A. J. A. de Oliveira, V. H. Etgens, *Phys. Rev. B* **82**, 094436 (2010).

10. J. Shin, A. Goyal, C. Cantoni, J. W. Sinclair, J. R. Thompson, *Nanotechnology* **23**, 155602 (2012).

11. F. Vidal, Y. Zheng, P. Schio, F. J. Bonilla, M. Barturen, J. Milano, D. Demaille, E. Fonda, A. J. A. de Oliveira, V. H. Etgens, *Phys. Rev. Lett.* **109**, 117205 (2012).

12. F. J. Bonilla, A. Novikova, F. Vidal, Y. L. Zheng, E. Fonda, D. Demaille, V. Schuler, A. Coati, A. Vlad, Y. Garreau, M. Sauvage Simkin, Y. Dumont, S. Hidki, V. Etgens, *ACS Nano* **7**, 4022 (2013).

13. V. Schuler, F. J. Bonilla, D. Demaille, A. Coati, A. Vlad, Y. Garreau, M. Sauvage-Simkin, A. Novikova, E. Fonda, S. Hidki, V. Etgens, F. Vidal, Y. Zheng, *Nano Research* **8**, 1964 (2015).

14. V. Schuler, J. Milano, A. Coati, A. Vlad, M. Sauvage-Simkin, Y. Garreau, D. Demaille, S. Hidki, A. Novikova, E. Fonda, Y. Zheng, F. Vidal, *Nanotechnology* **27**, 495601 (2016).

15. S. Kawasaki, R. Takahashi, T. Yamamoto, M. Kobayashi, H. Kumigashira, J. Yoshinobu, F. Komori, A. Kudo, M. Lippmaa, *Nat. Commun.* **7**, 11818 (2016).

16. L. Li, L. Sun, J. S. Gomez-Diaz, N. L. Hogan, P. Lu, F. Khatkhatay, W. Zhang, J. Jian, J. Huang, Q. Su, M. Fan, C. Jacob, J. Li, X. Zhang, Q. Jia, M. Sheldon, A. Alu, X. Li, H. Wang, *Nano Lett.* **16**, 3936 (2016).

17. J. Huang, L. Li, P. Lu, Z. Qi, X. Sun, X. Zhang, H. Wang, *Nanoscale* **9**, 7970 (2017).

18. Q. Su, W. Zhang, P. Lu, S. Fang, F. Khatkhatay, J. Jian, L. Li, F. Chen, X. Zhang, J. L. MacManus-Driscoll, A. Chen, Q. Jia, H. Wang, *ACS Applied Materials & Interfaces* **8**, 20283 (2016).

19. B. Zhang, M. Fan, L. Li, J. Jian, J. Huang, H. Wang, M. Kalaswad, H. Wang *Appl. Phys. Lett.* **112**, 013104 (2018).

20. M. Lee, R. Arras, R. Takahashi, B. Warot-Fonrose, H. Daimon, M.-J. Casanove, M. Lippmaa, *ACS Omega* **3**, 2169 (2018).

21. M. Hennes, V. Schuler, X. Weng, J. Buchwald, D. Demaille, Y. Zheng, F. Vidal, *Nanoscale* **10**, 7666 (2018).

22. X. Weng, M. Hennes, A. Coati, A. Vlad, Y. Garreau, M. Sauvage-Simkin, E. Fonda, G. Patriarche, D. Demaille, F. Vidal, Y. Zheng, *Phys. Rev. Materials* **2**, 106003 (2018).

23. M. Hennes, X. Weng, E. Fonda, B. Gallas, G. Patriarche, D. Demaille, Y. Zheng, F. Vidal, *Phys. Rev. Materials* **3,** 035002 (2019).

24. G. Radtke, M. Hennes, M. Bugnet, Q. M. Ramasse, X. Weng, D. Demaille, B. Gobaut, P. Ohresser, E. Otero, F. Choueikani, A. Juhin, Ph. Sainctavit, Y. Zheng, F. Vidal, *Advanced Materials Interfaces*, **6**, 1900549 (2019).

25. M. Lippmaa, S. Kawasaki, R. Takahashi, T. Yamamoto, *Jpn. J. Appl. Phys.* **59**, 010501 (2020).

26. B. Zhang, J. Huang, B. X. Rutherford, P. Lu, S. Misra, M. Kalaswad, Z. He, X. Gao, X. Sun, L. Li, H. Wang, *Materials Today Nano* **11**, 100083 (2020).

27. X. Weng, M. Hennes, T. Tran, N. Casaretto, D. Demaille, F. Vidal, Y. Zheng, *Cryst Eng. Commun.* **22**, 4730 (2020).

28. J. Huang, J. L. MacManus-Driscoll, H. Wang, *J. Mater. Res.* **32**, 1 (2017).

29. J. L. Mac Manus-Driscoll, P. Zerrer, H. Wang, H. Yang, J. Yoon, A. Fouchet, R. Yu, M. G. Blamire, Q. Jia, *Nature Materials* **7**, 314-320 (2008).

30. A. Chen, J.-M. Hu, P. Lu, T. Yang, W. Zhang, L. Li, T. Ahmed, E. Enriquez, M. Weigand, Q. Su, H. Wang, J.-X. Zhu, J. L. MacManus-Driscoll, L.-Q. Chen, D. Yarotski, Q. Jia, *Science Advances* **2**, e1600245 (2016).

31. D. Zhou, W. Sigle, M. Kelsch, H.-U. Habermeier, P. A. van Aken, *Adv. Mater. Interfaces* **2**, 1500377 (2015).

32. B. Zhang, J. Huang, B. X. Rutherford, P. Lu, S. Misra, M. Kalaswad, Z. He, X. Gao, X. Sun, L. Li, H. Wang, *Materials Today Advances* **8**, 100112 (2020).

33. R. Ferrando, J. Jellinek, R. L. Johnston, *Chem. Rev.* **108**, 845 (2008).

34. R. Ferrando, *Structure and Properties of Nanoalloys*, Volume 10, 1st Edition (Elsevier, 2016).

35. R. Ferrando, *J. Nanopart. Res.* **20**, 179 (2018).

36. D. Bochicchio, R. Ferrando, E. Panizon, G. Rossi, *J. Phys. Condens. Matter* **28**, 064005 (2016).

37. P. Lu, E. Romero, S. Lee, J. MacManus-Driscoll, Q. Jia, *Microscopy and Microanalysis* **20**, 1782 (2014).

38. D. H. Kim, X. Y. Sun, N. M. Aimon, J. J. Kim, M. J. Campion, H. L. Tuller, L. Kornblum, F. J. Walker, C. H. Ahn, C. A. Ross, *Advanced Functional Materials* **25**, 3091 (2015).

39. E. Enriquez, Q. Li, P. Bowlan, P. Lu, B. Zhang, L. Li, H. Wang, A. J. Taylor, D. Yarotski, R. P. Prasankumar, S. V. Kalinin, Q. Jia, A. Chen, *Nanoscale* **12**, 18193 (2020).

40. J. Buchwald M. Hennes, *Surf. Sci.* **701,** 121683 (2020).

41. A. Watanabe, Y. Kotake, Y. Kamata, A. Chikamatsu, K. Ueno, H. Misawa, T. Hasegawa, *J. Phys. Chem. Lett.* **5**, 25 (2014).

42. A. Watanabe, K. Ikemiya, A. Chikamatsu, Y. Hirose, T. Hasegawa, *Chem. Lett.* **43**, 225 (2014).

43. S. Misra, L. Li, D. Zhang, J. Jian, Z. Qi, M. Fan, H.-T. Chen, X. Zhang, H. Wang, *Adv. Mater.* **31**, 1806529 (2019).

44. J. Margueritat, J. Gonzalo, C. N. Afonso, A. Mlayah, D. B. Murray, L. Saviot, *Nano Lett.* **6**, 2037 (2006).

45. J. Margueritat, J. Gonzalo, C. N. Afonso, *Appl. Phys. Lett.* **88**, 093107 (2006).

46. M. Kalaswad, D. Zhang, X. Gao, L. Lopez Contreras, H. Wang, X. Wang, H. Wang, *ACS Appl. Mater. Interfaces* **11**, 45199 (2019).

47. D. Bossini, V. I. Belotelov, A. K. Zvezdin, A. N. Kalish, A. V. Kimel, *ACS Photonics* **3**, 1385 (2016).

48. K. Ikemiya, K. Konishi, E. Fujii, T. Kogure, M. Kuwata-Gonokami, T. Hasegawa, *Opt. Mater. Express* **4**, 1564 (2014).

49. E. Beaurepaire, J.-C. Merle, A. Daunois, J.-Y. Bigot, *Phys. Rev. Lett.* **76**, 4250 (1996).

50. C. D. Stanciu, F. Hansteen, A. V. Kimel, A. Kirilyuk, A. Tsukamoto, A. Itoh, Th. Rasing, *Phys. Rev. Lett.* **99**, 047601 (2007).

Figure Captions

Figure 1. Schematic illustration of a VAN and of the possibilities of magnetic anisotropy control.

Figure 2. (a) Axial strain $<\varepsilon_{zz}>$ as a function of NW diameter in Ni-CeO_2 VANs (disks, adapted from Ref. 13 by permission from Springer Nature Customer Service Centre GmbH: Springer Nature, Nano Research, Huge metastable axial strain in ultrathin heteroepitaxial vertically aligned nanowires, V. Schuler, F. J. Bonilla, D. Demaille, A. Coati, A. Vlad, Y. Garreau, M. Sauvage-Simkin, A. Novikova, E. Fonda, S. Hidki, V. Etgens, F. Vidal, Y. Zheng, © 2015) and Ni-STO VANs (triangles, adapted from Ref. 22 with permission). (b) Out-of-plane lattice parameters a_z of Co_xNi_{1-x}-STO VANs, with the cyan line as guide to the eye and the red line representing the bulk CoNi alloy reference [Ref. 27] - Reproduced by permission of The Royal Society of Chemistry. (c) Cross section transmission electron microscopy image of Ni nanowires in $SrTiO_3$ matrix; insets: Fast Fourier Transform of selected areas delimited by light squares. The inset at the top evidences the local misorientation α of the Ni lattice with respect to the $SrTiO_3$ lattice (reproduced from Ref. 22 with permission).

Figure 3.

(a-c) Magnetic hysteresis cycles at 10 K in Ni-STO (a), in Ni-CeO_2 (b) and in $Co_{0.2}Ni_{0.8}$-(BaSr)TiO_3 (c). (d) Magnetic hysteresis cycles at 300 K in a $Co_{0.63}Ni_{0.37}$-CeO_2 VAN. (e) Black line: Magnetostatic anisotropy at low temperature as a function of the Co content in Co_xNi_{1-x} alloy. Black triangle: magnetic anisotropy of Ni wires in Ni-CeO_2 VAN. K_{eff}, magnetic anisotropy extracted from magnetometry, of $Co_{0.32}Ni_{0.68}$ (green plain square, T = 10 K; open square, T = 300 K) and $Co_{0.63}Ni_{0.37}$ (dark red disk, T = 10 K; circle, T = 300 K) nanowires assemblies embedded in CeO_2. (a) adapted from Ref. 24 with

permission. (b,d,e) adapted from Ref. 12 “Combinatorial Growth and Anisotropy Control of Self-Assembled Epitaxial Ultrathin Alloy Nanowires”, F. J. Bonilla, A. Novikova, F. Vidal, Y. L. Zheng, E. Fonda, D. Demaille, V. Schuler, A. Coati, A. Vlad, Y. Garreau, M. Sauvage Simkin, Y. Dumont, S. Hidki, V. Etgens, ACS Nano 7, 4022 (2013). Copyright 2013 American Chemical Society. (c) adapted from Ref. 14, doi.org/10.1088/0957-4484/27/49/495601 © IOP Publishing. Reproduced with permission. All rights reserved).

Figure 4. (a) VANs with nanowires exhibiting core-shell (CS) multilayer, and bilayer segregation patterns. (b) Hybrid Au-Co-$SrTiO_3$ VAN: STEM-HAADF and EDX chemical mapping of Co and Au in cross-sectional view. Reproduced from Ref. 23 with permission.

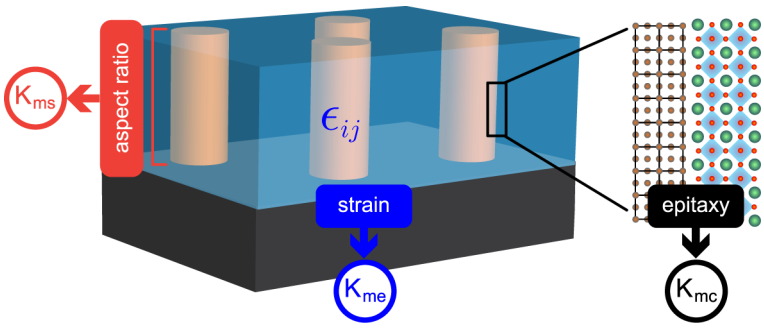

FIG. 1

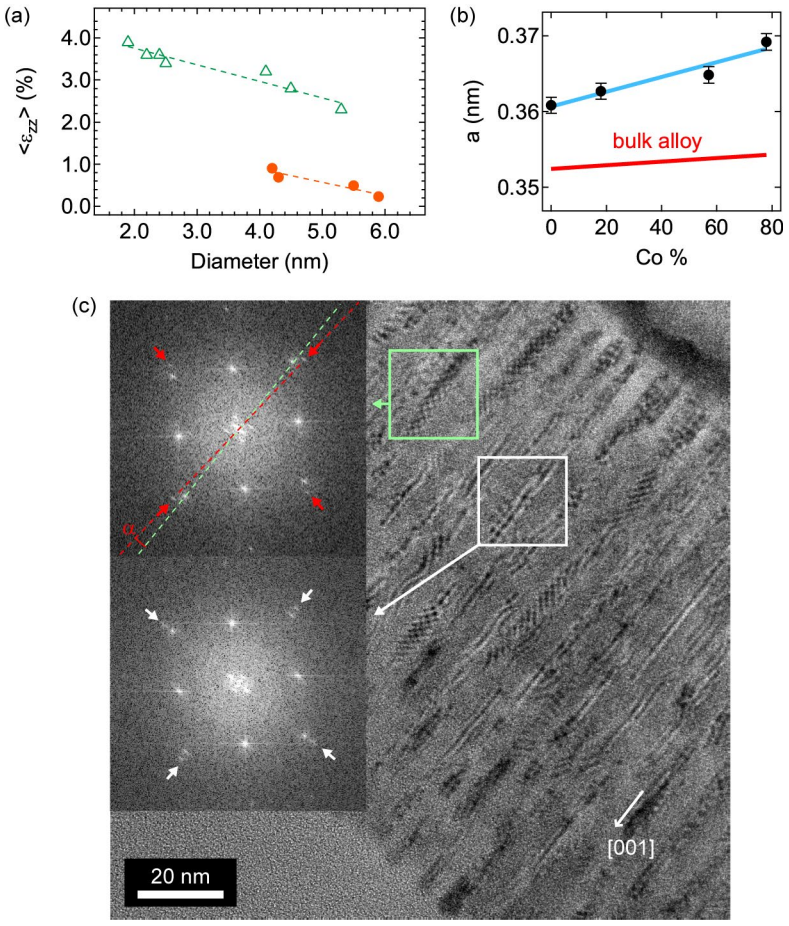
(a)
<ε_zz> (%)
4.0
3.0
2.0
1.0
0.0
2.0
3.0
4.0
5.0
6.0
Diameter (nm)
(b)
a (nm)
0.37
0.36
0.35
bulk alloy
0
20
40
60
80
Co %
(c)
20 nm
[001]

FIG. 2

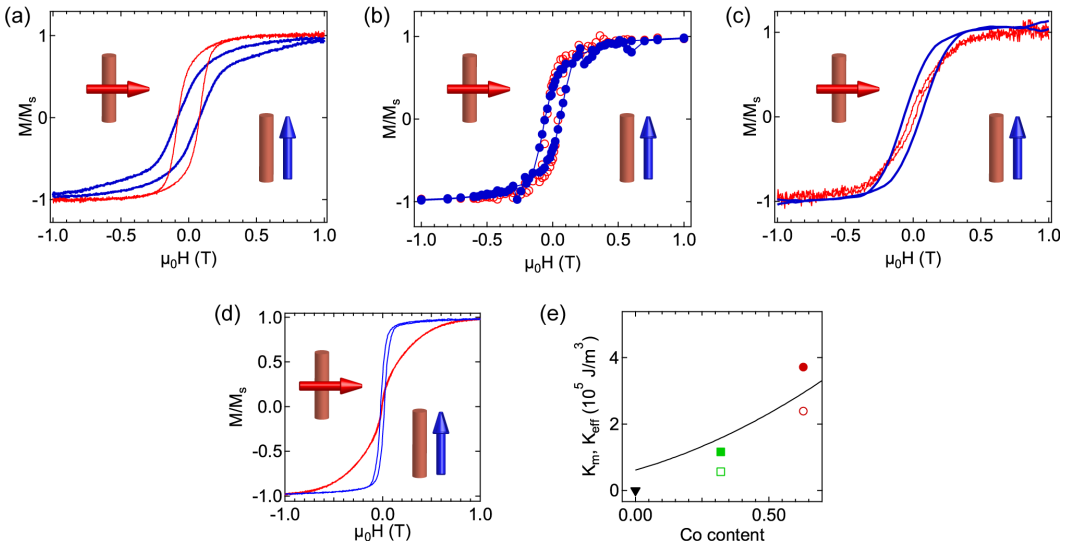

FIG. 3

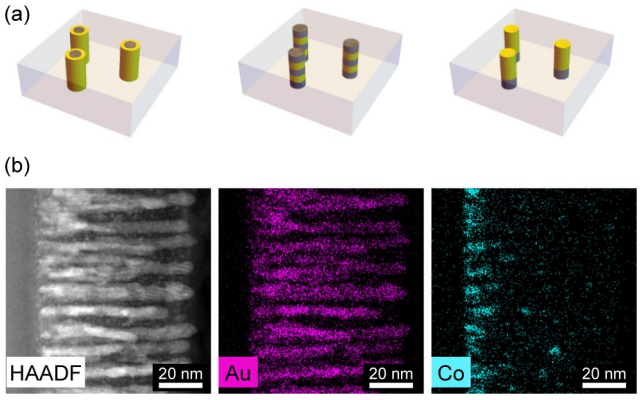

FIG. 4